Immunological tolerance to luciferase and fluorescent proteins using tol mice enables development of improved tumor models for investigating immunity and metastasis

Khan, K.A.; Qureshi, A.A.; Xu, P.; Kuo, H.Y.; Schumacher, T.N.; Michael, I.P.; Kerbel, R.S.

Immunological Tolerance to Luciferase and Fluorescent Proteins Using Tol Mice Enables Development of Improved Tumor Models for Investigating Immunity and Metastasis

Kabir A. Khan[1,2], Areeba A. Qureshi[1,2], Ping Xu[1,2], Hung-Yang Kuo[3], Ton N. Schumacher[4,5], Iacovos P. Michael[1,2], and Robert S. Kerbel[1,2]

ABSTRACT

There is a continuing need for improved preclinical mouse models of cancer that more accurately predict therapy outcomes for future clinical translation. Luciferase and bioluminescence have long been utilized to generate models conducive to noninvasive imaging to monitor tumor growth, disease progression, and response to therapy. However, luciferase, as well as fluorescent reporter proteins, are highly immunogenic, limiting their use in some syngeneic tumor models in immunocompetent mice. In this study, we described the utility of transgenic mice engineered to have tolerance to luciferase and several other reporter proteins, known as Tol mice, in cancer immunology research. Some tumor cell lines expressing both luciferase and GFP were completely rejected in wild-type mice but maintained robust growth in Tol mice. Additionally, Tol mice allowed the development of an experimental brain metastasis model and a postsurgical resection spontaneous metastasis model. Importantly, even when certain cell lines carrying reporter proteins successfully formed tumors in immunocompetent wild-type mice, underlying immunity existed that could be reinvigorated by immune checkpoint inhibitors. Therefore, caution is needed when using such models in wild-type mice, as exaggerated effects may be induced by immunotherapy. Tol mice circumvent this problem and will likely widen the number of orthotopic and metastatic tumor models that can be used in immunotherapy studies in both C57Bl/6 and BALB/c mice.

Significance: Tol transgenic mice, tolerant to reporter proteins like luciferase and GFP, can be used to develop improved tumor models for studying metastasis and immunotherapy, avoiding immune rejection issues in immunocompetent mice.

See related commentary by Grzelak and Ghajar, p. 2143

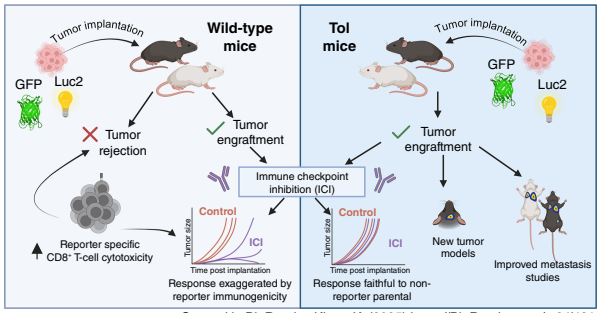

Created in BioRender. Khan, K. (2025) https://BioRender.com/m24i181

Introduction

Immunotherapy of cancer continues to be at the forefront of cancer research and treatment, with a considerable number of treatments being evaluated, particularly those targeting the immune checkpoint molecules PD-1 or PD-L1, often combined with other therapeutic modalities (1). However, in some situations, there can be little rationale for testing certain combination therapies in clinical trials, and robust prior reports of preclinical testing are often lacking to aid the justification of undertaking large and expensive clinical trials, especially at the phase III level, many of which have failed (2). There are many challenges in the tumor immunotherapy field and 10 such challenges were summarized by Hegde and Chen (3). This study aims to address one of these challenges – the need for better preclinical models. There are many problems with preclinical models not translating well (or at all) to clinical scenarios. One such problem has been described extensively elsewhere and involves the most common situation of treating only primary and sometimes exclusively subcutaneous tumors (4, 5). The use of orthotopic tumor implantation and modeling of metastatic disease better replicates clinical scenarios with higher predictive potential. Luciferase-based bioluminescence has been used extensively in studies to visualize internal primary tumors and metastases. Indeed, the first use of luciferase for this purpose was carried out in 1994 (6). Many studies utilizing the imaging strategy have been published, with most involving human tumor xenografts in immunocompromised mice, in which immunogenicity of luciferase was of little or no concern.

Reporter proteins such as luciferase and GFP have long been known to be immunogenic when expressed ectopically in immunocompetent

[1]Department of Medical Biophysics, University of Toronto, Toronto, Canada. [2]Biological Sciences Platform, Sunnybrook Research Institute, Toronto, Canada. [3]Department of Oncology, Graduate Institute of Oncology, National Taiwan University Hospital, National Taiwan University College of Medicine, Taipei, Taiwan. [4]Division of Molecular Oncology and Immunology, Oncode Institute, The Netherlands Cancer Institute, Amsterdam, the Netherlands. [5]Department of Hematology, Leiden University Medical Center, Leiden, the Netherlands.

Corresponding Authors: Kabir A. Khan, Sunnybrook Research Institute, S-221 Research Building, 2075 Bayview Avenue, Toronto M4N 3M5, Ontario, Canada. E-mail: kkhan@sri.utoronto.ca or kabirkhanphd@gmail.com; and Robert S. Kerbel, Sunnybrook Research Institute, S-217 Research Building, 2075 Bayview Avenue, Toronto M4N 3M5, Ontario, Canada. E-mail: robert.kerbel@sri.utoronto.ca or rskerbel@gmail.com

Cancer Res 2025;85:2165–78

doi: 10.1158/0008-5472.CAN-24-2418

mice, and the immunodominant epitopes capable of being presented to $CD8^+$ T cells by MHC class I have been identified in both C57Bl/6 and BALB/c mice (7–9). Such immunogenicity of luciferase or GFP or both has been shown to result in the rejection of tumor cells in some models (10–15). Others have shown reductions in the extent of metastasis (16).

Here, we describe the use of transgenic "Tol" mice, which were previously generated to maintain immunologic tolerance against a range of reporter and modifier proteins (17). These include AzGreen, Kaede, Katushka, mKO2, TagBFP, enhanced GFP (eGFP), luciferase 2 (Luc2), and Cre recombinase. Immunologic tolerance was generated by the use of a "Tolerizer" expression cassette, which contained N-terminal and C-terminal portions of each gene shuffled to create nonfunctional proteins but that contained all necessary epitopes for recognition by the adaptive immune system as self-antigens. It was previously shown that the adoptive transfer of $CD8^+$ T cells expressing certain fluorescent proteins present in the Tolerizer cassette allowed extended maintenance in Tol mice in comparison with wild-type mice (WT; ref. 17). Here, we describe for the first time the comparison of Luc2- and GFP-transduced tumor cells implanted into WT versus Tol mice. In some cases, the tumor cells are completely rejected in WT whereas they are maintained in Tol mice. In other cases, the cells are maintained in both mouse strains but grow slower in WT mice. Importantly, we demonstrate that Tol mice can be used to develop models of postsurgical metastatic disease, as shown in the triple-negative breast cancer 4T1.2 line, as well as experimental brain metastasis via direct injection into the Tol mouse brain. We also show that luciferase staining can be used as a way of identifying tumor cells. Finally, we demonstrate that even in settings in which luciferase- and GFP-expressing cells such as B16 melanoma grow in both WT and Tol mice, major differences are observed between these mice when undergoing immunotherapy, with WT showing higher numbers of complete responses (CR), whereas little therapeutic efficacy is detected in Tol mice.

Materials and Methods

Cells

E0771 breast cancer cells (biological sex female) were obtained from ATCC (RRID: CVCL_GR23). B16F1 melanoma (RRID: CVCL_0158; biological sex male) cells were obtained from the late Dr. Isaiah J. Fidler. 4T1.2 (RRID: CVCL_GR32; biological sex female) breast cancer cells were obtained from Dr. Robin L Anderson (University of Melbourne, Melbourne, Australia; ref. 18). Cell line authentication was not performed but early-passage vials were returned to and cultured for three to four passages. Mouse tumor cell lines were cultured in DMEM with 5% FCS. After cell sorting, cells were cultured for at least two passages in media containing penicillin, streptomycin, and fungizone. HEK293T cells (RRID: CVCL_0063; courtesy of Dr. David Andrews' lab) were cultured in DMEM with 10% FCS. Cells were screened for *Mycoplasma* and other pathogens and confirmed to be negative by the Mouse Essential CLEAR Infectious Disease PCR (Charles River Laboratories) or by in-house *Mycoplasma* screening PCR using a nine-primer pool (19).

Plasmids and constructs

The minimal ubiquitous chromatin-opening element (UCOE) from the human CBX3 promoter was amplified from the pMH0006 plasmid (a gift from Martin Kampmann and Jonathan Weissman; Addgene, plasmid #135448, RRID: Addgene_135448) using the primers aagaccaccgcacagcaagcgcggccgcTGATCTTCAGACCTGGAGG (forward) and caggcaccagagcaggccggggccggccAGCTTGAGACTACCCCCG (reverse) and then Gibson-cloned (Gibson Assembly Master Mix, New England Biolabs #E2611S) into pWPi (a gift from Didier Trono; RRID: Addgene_12254) between restriction sites NotI and FseI to create the pLUEF1 IRES GFP lentiviral vector (Addgene #224466). Luc2 was amplified from the pFU Luc2-eGFP plasmid (a gift from Professor Jennifer Prescher), using primers cgagactagcctcgaggtttaaacATGGAAGATGCCAAAAAC (forward) and attcctgcagcccgtagtttaaacTTATTACACGGCGATCTTG (reverse) and Gibson-cloned into pLUEF1-IRES-GFP between PmeI restriction sites, to create pLUEF1-Luc2-IRES-GFP (Addgene #224467). The packaging and envelope plasmids psPax2 and pMD2.G were used in cotransfection to create lentiviral particles (gifts from Didier Trono; RRID: Addgene 12260 and Addgene 12259). All plasmids were confirmed to be of the correct sequence by Sanger sequencing (The Centre for Applied Genomics, Toronto, Ontario, Canada).

Lentiviral transductions

As described previously (20), briefly, HEK293T cells (3×10^6 in a 10-cm plate) were transfected with 9 μg total plasmid DNA of pLUEF1, psPax2, and pMD2.G vectors at a ratio of 3.3:2.5:1 using polyethylenimine (average molecular weight ~25,000, branched; Sigma-Aldrich #408727) at a ratio of 1:4 DNA to polyethylenimine. The next day, media from two 10-cm plates were changed, and 48 hours later, viral media were collected, centrifuged, and passed through a 0.45-μm sterile filter and applied to 500,000 target cells plated in T75 flasks in the presence of 8 μg/mL of polybrene (Sigma, hexadimethrine bromide #H9268). Two days later, the medium was changed for a second round of transduction, and flow cytometry was performed 2 days later to determine transduction efficiency.

Flow cytometry and FACS

Lentiviral transduction efficiency (% GFP+) was analyzed in comparison with nontransduced cells using an LSR II (BD Biosciences). After multiple passages to ensure stable integration of the transgene, the top 10% GFP+ cells were sorted using a BD FACSAria Fusion cell sorter and then cultured for at least three passages, expanded, and frozen down. Similar passages were used for all implantation experiments.

Breeding mice

Sperm from Col1a1$^{tm23(CAG\text{-}Tol,\text{-}cre)NKI}$ (MGI ID: 6342020) mice was used to artificially inseminate WT C57Bl/6 females (The Jackson Laboratory). Heterozygote pups were bred together and then backcrossed to naïve WT C57Bl/6 females every 6 months to avoid genetic drift. Tol C57Bl/6 males and females were bred with WT BALB/c females or males (The Jackson Laboratory). Mice were genotyped using a three-primer PCR using Taq DNA polymerase (GenScript #E00007) using primers mouse genomic DNA (gDNA) wt1 forward GCCATCCCAACAATACATCA, mouse gDNA wt2 reverse TGGTTTCTTTGGGCTAGAGG, and Tol MRT insert BGH forward TAGTTGCCAGCCATCTGTTG to amplify a region in the gDNA flanking in which the Tol cassette inserts (for identification of WT) or a region spanning the C-terminus of the Tol cassette and genomic DNA in the Col1a1 locus (for identification of Tol); therefore, differences in sizes would be able to distinguish between WT, heterozygotes, and homozygotes (See Supplementary Fig. S1A and S1B). Age-matched WT and Tol heterozygotes were used for all experiments from in-house breeding colonies, and littermate controls were used where possible.

Mammary fat pad and subcutaneous tumor implantations

All animal experiments were carried out with the approval of the institutional Animal Care Committee of Sunnybrook Research Institute in accordance with the Canadian Council on Animal Care guidelines. B16F1-Luc2/GFP cells (200,000) were implanted subcutaneously (30G needle) into the left or right flank of male Tol or WT mice aged 8 to 16 weeks. E0771 parental (E0771P) or E0771-Luc2/GFP cells (500,000) were injected (30G needle) in the mammary fat pad as described previously for female Tol or WT mice aged 8 to 16 weeks (21). As a method to stimulate tumor immunity, 10 million E0771-Luc2/GFP cells were lethally irradiated with a 50 Gy dose of ionizing radiation in a T75 flask *in vitro* using a Faxitron X-ray Irradiator (Faxitron). Two days after irradiation, 500,000 cells were implanted in the mammary fat pad. For tumor rechallenges, the original number of nonirradiated cells was used for implantation, albeit on the opposite side of the mouse; alternatively, a 1- to 2-mm diameter tumor piece was implanted by creating a small pocket in the mammary fat pad and such tumor fragments were from E0771-Luc2/GFP tumors originally grown in Tol mice. For surgical resections, at 15 days post implantation (DPI), mice were depilated at the tumor site, the chest, and abdomen. The primary tumor was resected along with surrounding mammary fat pad tissue and laid in a petri dish containing 300 μg/mL of D-luciferin in PBS and subjected to bioluminescence imaging (BLI). Primary tumors were measured using Vernier calipers.

Brain implantation

E0771-Luc2/GFP cells (100,000) were stereotactically implanted into the right caudate-putamen ($x = 2$ mm, $y = 0$ mm, and $z = -3$ mm) of female Tol or WT C57Bl/6 mice aged 10 to 14 weeks, at a rate of 100 nL per minute (2 μL total volume) using a Hamilton syringe and 30G needle. Per experiment, a maximum of four mice could be implanted each day; hence, implantations were carried out over 2 days to include two WT and two Tol mice each day. Data from two separate experiments were pooled for survival analyses and tumor occurrence.

Immunotherapy treatments

On day 12 after implantation, mice bearing B16F1-Luc2/GFP melanoma were separated into treatment groups to ensure similar mean tumor volume in each group. Mice were intraperitoneally injected with 150 μg mouse CTLA4 antibody clone 9D9 (Bio X Cell, cat. #BP0164, RRID: AB_10949609), 250 μg of PD-1 antibody, murinized RecombiMAb with D265A mutation from clone RMP1-14-CP151 (Bio X Cell, cat. #CP151, RRID: AB_2927525), or mouse isotype control antibody (Bio X Cell, cat. #BE0086, RRID: AB_1107791).

BLI

Mice were intraperitoneally injected with 150 mg/kg of D-luciferin dissolved in PBS (IVISbrite D-Luciferin Potassium Salt bioluminescent substrate PerkinElmer/Revvity #122799) and imaged using the Newton 7.0 (Vilber) small animal imager. Data were acquired using the Evolution software (Vilber) and quantified using Kuant software (Vilber). BLI quantification was performed on images that did not show signal saturation. Regions of interest were drawn around areas of tumor and kept consistent between time point comparisons, and regions of interest were also used for background subtractions.

Enzymatic dissociation of tumors

Tumors were resected from mice, minced to fine pieces with a razor blade, and digested in an enzymatic solution containing 1% BSA, 12,500 units collagenase II (Worthington), 12,500 units collagenase IV (Worthington), and DNase I, 10 μg/mL (cat. #LS006333, Worthington) for 45 minutes at 37°C with gentle shaking. After neutralization in DMEM containing 10% FCS, digests were passed through a 70-μm cell strainer, and the cells were then cultured in the original media and GFP positivity was monitored.

Flow cytometry of peptide MHC tetramers in digested tumors

At 12 days after implantation, B16F1-Luc2/GFP tumors were excised from WT and Tol mice. After mincing with razor blades, tumors were transferred to the enzymatic solution described above. After dissociation, 1 million cells were used per stain and transferred to a 96-well deep well plate for all staining and washing steps (Corning #3960). Zombie violet fixable viability stain (BioLegend, # 423114) was incubated at 1:1,000 in PBS for 20 minutes in dark at room temperature. The cells were washed and then incubated for 30 minutes in FcR block anti-CD32/CD16 (1:100 dilution, 5 μg/mL; BD Biosciences, cat. #553142, RRID: AB_394657). The cells were washed and then incubated with fluorescent labeled pMHC tetramers for 45 minutes on ice (1:200 dilution). H2-Db DTLVNRIEL (GFP peptide 118–126) tetramer PE and H2-Db LMYRFEEEL [firefly luciferase (Luc2) peptide 264-272] APC or negative control H2-Db ASNENMETM (influenza A peptide) tetramer PE or negative control H2-Db ASNENMETM (influenza A peptide) APC (all obtained from the NIH Tetramer Facility) were used. The cells were washed again and then incubated with the following antibody panel: CD45 (clone 30F-11) BUV395 (1:100; BD Biosciences, cat. #565967, RRID: AB_2739420), CD8a (clone 53-6.7) BUV737 (BD Biosciences, cat. #612759, RRID: AB_2870090; 1:200), CD4 (clone GK1.5) PerCP Cy5.5 (1:200; BioLegend, cat. #100434, RRID: AB_893324), and PD-1 (clone 29F.1A12) PE-Cy7 (1:200; BioLegend, cat. #135216, RRID: AB_10689635) for 45 minutes on ice. The cells were then washed and fixed in paraformaldehyde for 10 minutes, washed, and stored overnight and analyzed 24 hours later using a BD FACSymphony A5 flow cytometer (BD Biosciences). Fluorescence minus one controls for antibodies were included and used for gating strategy. The following were gated on: single cells, live cells, $CD45^+$, $CD8a^+$, tetramer APC negative (for PE tetramers), and tetramer PE negative (for APC tetramers; gating schemes are provided as Supplementary Fig. S2). Negative control tetramers were used in separate conditions to determine background staining and were used for gating, allowing ~0.5%+ cells in each tetramer-positive gate. Compensation was determined using single stains of UltraComp eBeads (Thermo Fisher Scientific #01-2222-41). Data were analyzed using FlowJo v10.8.1 (RRID: SCR_008520).

Immunofluorescence of frozen sections

Tissues were frozen in optimal cutting temperature, lungs were inflated with a 1:1.5 optimal cutting temperature:PBS mix, and immunofluorescence was performed as described previously (22). Lung sections were cut at 12 μm and liver at 6 μm. After thawing, tissues were fixed on the slide with chilled methanol for 5 minutes and then blocked in Dako blocking buffer (Agilent, Dako #X0909) with 10% donkey serum for 30 minutes at room temperature. Brain sections were cut at 10 μm, thawed, fixed with chilled methanol for 10 minutes, and then blocked in PBS-Triton (0.1%) prepared in-house with 10% donkey serum for 1 hour at room temperature. Primary antibodies were incubated overnight at 4°C – endomucin

clone V.7C7 (Thermo Fisher Scientific, cat. #14-5851-82, RRID: AB_891527; 1:500 dilution, 1 μg/mL), CD31 FITC clone MEC13.3 (BioLegend, cat. #102506, RRID: AB_312913; 1:50 dilution, 10 μg/mL), luciferase goat polyclonal antibodies (R&D Systems/Novus, cat. #NB100-1677, RRID: AB_10000585; 1:500 dilution), and GFP chicken polyclonal antibody (Abcam, cat. #ab13970, RRID: AB_300798; 1:800). Secondary antibodies included Alexa Fluor 647 AffiniPure F(ab')$_2$ Fragment donkey anti–rat IgG (H+L; Jackson ImmunoResearch, cat. #712-606-153, RRID: AB_2340696; 1:500), donkey anti–goat IgG (H+L), highly cross-adsorbed CF750 (Biotium #20362; 1:500), and Rhodamine Red-X AffiniPure donkey anti–chicken IgY (IgG; H+L; Jackson ImmunoResearch, cat. #703-295-155, RRID: AB_2340371). Slides were stained with DAPI and mounted in ProLong Diamond and images were acquired on a Zeiss Axio Observer with Colibri LED light source. Whole-tissue sections were scanned and processing included stitching and shading correction (ZEN, Zeiss).

Statistical analysis

Statistical analyses were performed using Graphpad Prism 5.0. *P* values were derived from two-tailed unpaired Student *t* tests, and *P* values for survival analyses were derived with the log-rank Mantel–Cox test.

Data availability

The data generated in this study are available upon request from the corresponding author, K.A. Khan.

Results

Breast cancer cells coexpressing luciferase and GFP are rejected in WT mice but grow in Tol mice

Alongside the risk of rejection of luciferase- or GFP-expressing cells is the potential for bioluminescence signal to decrease *in vivo*; historically, we have detected loss of signal in two different orthotopic breast cancer models despite increases in tumor volume (Supplementary Fig. S3A–S3G). Such loss of expression could be due to tumor clones highly expressing luciferase being depleted by the adaptive immune system or perhaps the transgene becoming epigenetically silenced or lost due to chromosomal instability; additionally, loss of signal could be due to necrosis within a tumor (especially bioluminescence signal). To ensure that Luc2 and GFP were constitutively expressed upon passaging *in vitro* and proliferation *in vivo*, and to be less prone to epigenetic silencing, the lentiviral pLUEF1 (plasmid Lentiviral UCOE EF1α) vector was created, which contains a UCOE before the constitutively active EF1α promoter (**Fig. 1A**). The use of a UCOE has been shown to decrease promoter CpG methylation (23). The Luc2 gene was codon optimized for mammalian expression and cloned after the promoter and separated from eGFP (referred to as GFP henceforth) by an internal ribosome entry site (IRES) to allow simultaneous expression of each reporter protein. GFP was utilized to allow FACS of positive cells to maintain a higher level of heterogeneity than can be acquired with clonal selection and expansion. The E0771 mouse breast cancer cell line was transduced with this vector to generate Luc2 and GFP reporter cells; the double reporter cell lines are referred to as Luc2/

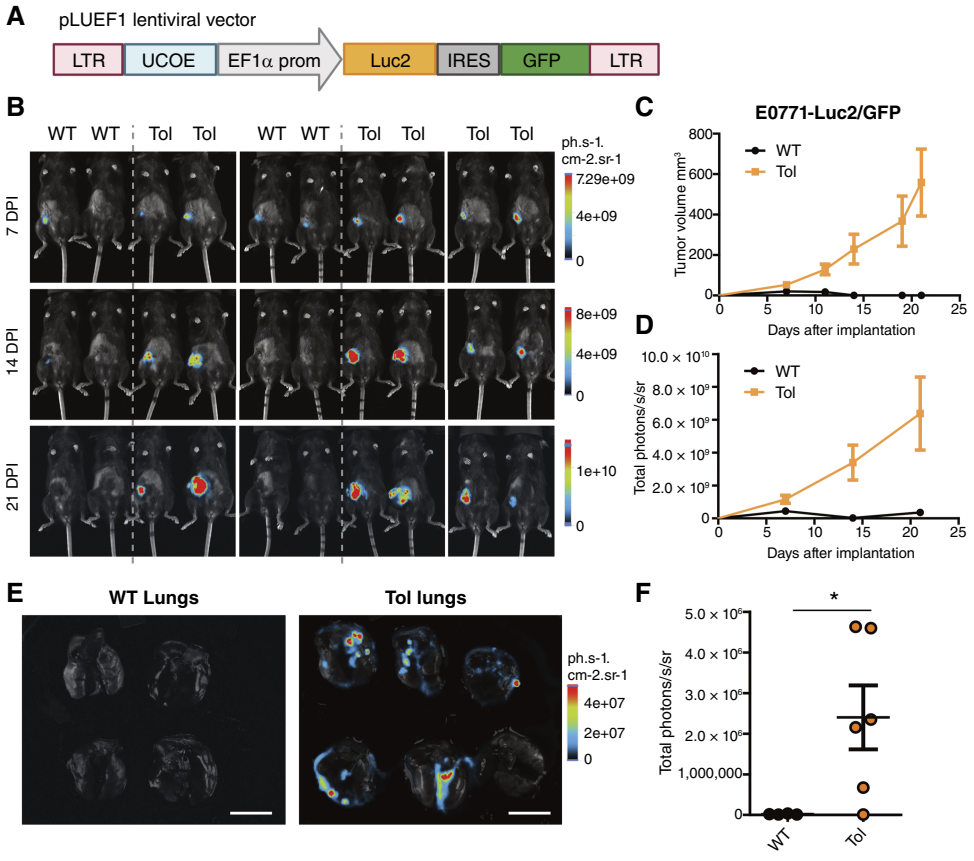

Figure 1.

E0771-Luc2/GFP tumor growth is maintained in Tol mice but rejected in WT mice. **A,** Schematic diagram of the pLUEF1 lentiviral vector. EF1α prom, EF1α promoter; IRES, internal ribosome entry site; LTR, long terminal repeats. **B,** BLI of WT vs. Tol mice used as recipients for implantation of E0771-Luc2/GFP cells. **C,** Tumor volume of mice from **B**. **D,** BLI quantification of mice from **B**. **E,** *Ex vivo* BLI of WT and Tol lungs. Scale bar, 1 cm. **F,** BLI quantification of lungs at endpoint, total photons per second per steradian. An unpaired *t* test was used. *, $P = 0.0416$. WT, $n = 4$; Tol, $n = 6$. sr, steradian.

GFP in the rest of the text. E0771-Luc2/GFP cells were used to determine capacity for tumor formation in WT or Tol mice. After implantation into the mammary fat pad, bioluminescent signal could be detected in all mice at 7 DPI (**Fig. 1B**). However, at 14 DPI, the majority of tumors in WT mice had been rejected and were undetectable (three of four mice); subsequently 21 days later, all WT mice had rejected the implanted tumor cells, but in contrast, in the Tol mice, formation of tumors was observed (**Fig. 1B-D**). Upon experimental endpoint, all lungs were visualized *ex vivo* by BLI, which revealed no detectable metastases in WT mice, whereas lung metastases could be observed in the Tol mice (five of six; **Fig. 1E** and **F**).

Tol mice can mount an adaptive immune response against E0771-Luc2/GFP breast cancer cells

To verify that the Tol mice maintain the ability to mount an adaptive immune response and that impaired immunity due to expression of the large Tol protein was not the reason for differences in the growth of E0771-Luc2/GFP tumors, an immunization-like approach was utilized. In short, we intended to raise an adaptive immune response against tumor cells that could not proliferate and then re-challenge with the original tumor line to determine whether an adaptive immune response was indeed generated, resulting in slower tumor growth or even complete rejection (**Fig. 2A**). Tol mice were used as recipients for orthotopic implantation with lethally irradiated E0771-Luc2/GFP cells in the mammary fat pad. BLI revealed that all cells in each implantation could emit bioluminescent signals on the day of implantation, demonstrating the presence of live cells that are presumably unable to proliferate (**Fig. 2B**). After 4 weeks of observation, no tumors grew from the irradiated E0771-Luc2/GFP cells. To determine whether this single-dose immunization was sufficient to confer adaptive immunity, four mice were rechallenged with nonirradiated E0771-Luc2/GFP cells, and four separate mice were rechallenged with E0771-Luc2/GFP tumor fragments (1–2 mm in diameter), both implantations being in the contralateral mammary fat pad. Tumor fragments were derived from tumors originally grown in the mammary fat pad of Tol mice and were used to determine whether an immune response could be raised against a larger established tumor. In mice rechallenged with E0771-Luc2/GFP cells, BLI signal was present in all mice on days 1 and 9 after rechallenge (**Fig. 2B**). Eventually each group of mice rejected two of four rechallenges (**Fig. 2C** and **D**) of cells or tissue. In addition, the growth kinetics for the tumors that did grow from cell rechallenges were considerably slower when compared with E0771-Luc2/GFP cells implanted into naïve Tol mice (**Fig. 2E**), demonstrating that Tol mice are indeed capable of launching an adaptive immune response against this tumor. Although this does not unequivocally prove that rejection is raised against intrinsic E0771 tumor antigens, we and others have shown previously that E0771 parental cells respond and undergo complete regressions in response to ICIs, supporting the presence of strong tumor antigens (24, 25).

Melanoma B16F1-Luc2/GFP cells display reduced primary tumor growth and metastasis and increased GFP- and Luc2-specific CD8$^+$ T cells in WT versus Tol mice

In order to determine whether a less immunogenic cell line would result in similar findings to E0771 results, we chose the mouse B16F1 melanoma cell line, which we have previously shown to not respond well to PD-L1 antibody monotherapy (26). B16F1 cells were transduced with the same pLUEF1 Luc2-IRES-GFP construct and implanted into WT versus Tol mice, which resulted in a significant reduction in tumor size and growth rate in WT mice compared with Tol, as well as a reduction in BLI signal (**Fig. 3A** and **B**). The BLI signal in the core of large tumors was reduced at later time points (15 DPI and beyond) in both WT and Tol mice, likely because of necrosis in the tumor center (**Fig. 3B**; Supplementary Fig. S4A).

To investigate the presence of GFP- and luciferase-specific cytotoxic T-cell responses, we utilized peptide MHC class I tetramer staining using the immunodominant peptides of GFP (DTLVNRIEL) and luciferase (LMYRFEEEL) in C57Bl/6 mice (Supplementary Fig. S4B; refs. 8, 9). B16F1-Luc2/GFP tumors were dissociated after 12 days of growth in WT versus Tol mice and flow cytometry was performed. The mean fluorescence intensity of GFP in CD45-negative cells (used as a surrogate for tumor cells but will also include GFP-negative nontumor stromal cells) was significantly reduced in WT mice compared with Tol, consistent with the possibility of high GFP expressors being eliminated by the adaptive immune system (**Fig. 3C**). Additionally, levels of intratumoral CD8$^+$ T cells in WT mice were significantly higher than Tol mice, suggesting activation and expansion in WT versus Tol mice (**Fig. 3D**). Indeed, PD-1$^+$ CD8$^+$ T cells were significantly higher in WT versus Tol, suggesting the potential of increased activation (Supplementary Fig. S4C). To determine the levels of antigen-specific CD8$^+$ T cells and add another layer of specificity, we utilized PD-1 expression to identify PD-1$^+$ tetramer+ activated CD8$^+$ T cells (Supplementary Fig. S4B). This revealed significantly more GFP- (**Fig. 3E**) and luciferase-specific (**Fig. 3F**) CD8$^+$ T cells in WT than in Tol mice; this was also the case for absolute numbers (Supplementary Fig. S4D). Similar differences were observed for all GFP and luciferase tetramer–positive CD8$^+$ T cells irrespective of activation status (Supplementary Fig. S4E). These data suggest that Tol mice display tolerance to GFP and luciferase and do not mount a robust and specific immune response as observed in WT mice.

To determine whether similar findings as observed in primary tumors could be seen in metastatic settings, B16F1-Luc2/GFP cells were injected into the tail vein of WT versus Tol mice. The majority of mice displayed signal 1 hour after injection, mainly in the lungs; however, there was no significant difference between WT and Tol at this point (Supplementary Fig. S4F). Over several weeks, Tol mice developed extensive metastases as visualized by BLI and displayed symptoms of disease burden sooner than the majority of WT mice (**Fig. 3G**). This was reflected in survival analyses of WT versus Tol mice (**Fig. 3H**) and BLI quantification (**Fig. 3I**). The slower development of both primary tumors and metastases in WT mice suggests that an adaptive immune response is raised in WT but not in Tol mice.

Luciferase can be utilized as a tumor-specific marker by immunostaining in Tol mice

Many mouse tumor cell lines lack robust tumor-specific markers that can be identified in downstream histology or flow cytometry analyses. One of the many major benefits of utilizing a tumor model that expresses a trackable or reporter protein is exploiting its use as a tumor-specific marker, especially in histologic analyses. However, as the Tol mice technically contain epitopes for luciferase in every cell, it was unclear whether immunostaining of luciferase or other reporter proteins could be successfully performed. Therefore, we conducted immunostaining on lungs and livers containing B16F1-Luc2/GFP tumors. Metastatic sites were chosen to compare tumor lesions against normal healthy tissue in the same tissue section. Vessels were

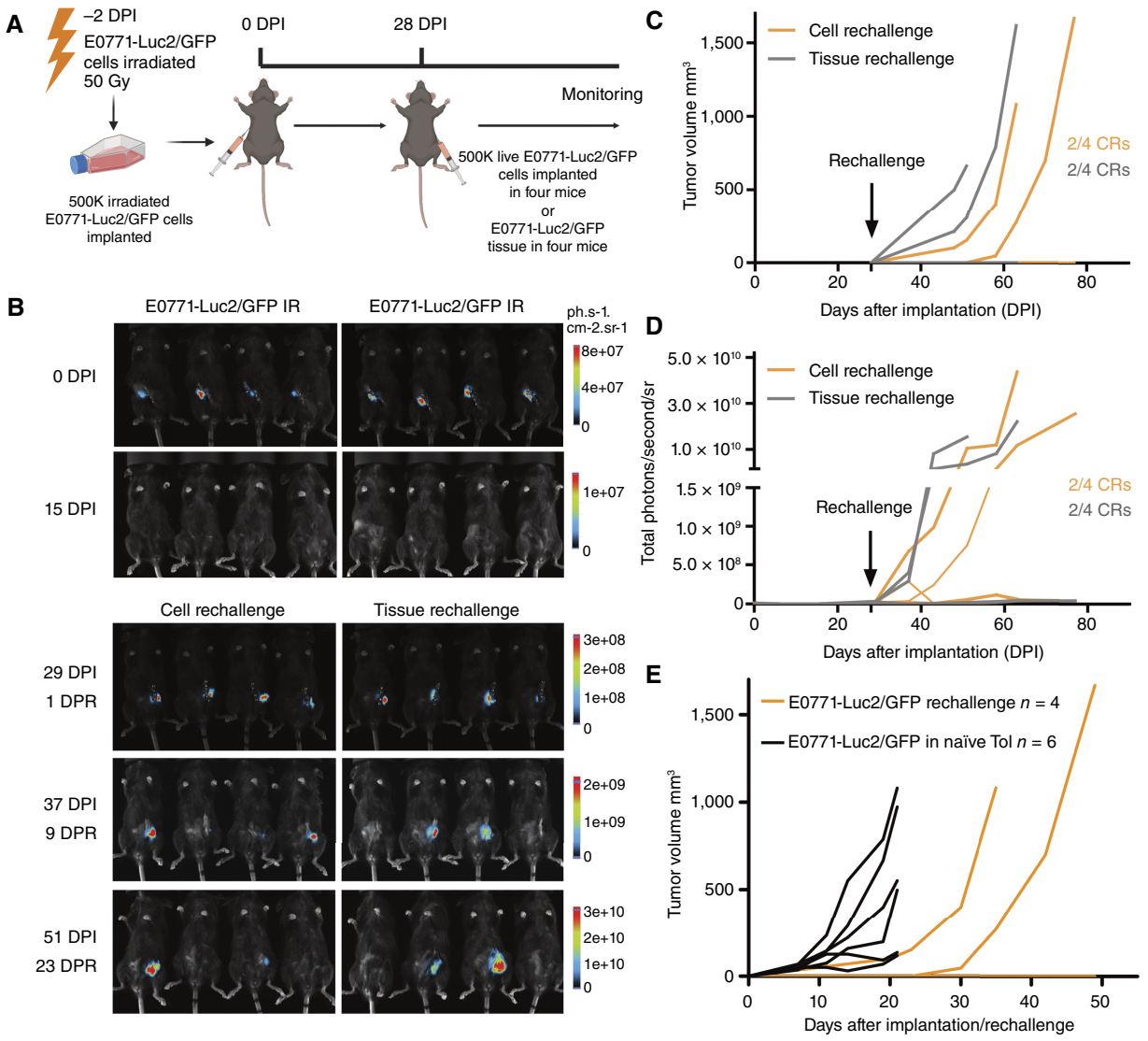

Figure 2.

E0771-Luc2/GFP irradiated cell implantation in Tol mice to test capability of the adaptive immune system. **A,** Schematic diagram of the experimental design. **B,** BLI of Tol mice implanted with irradiated E0771-Luc2/GFP at 0 DPI and then rechallenged with nonirradiated E0771-Luc2/GFP either as cells or tumor tissue fragments. DPR, days post rechallenge. **C,** Tumor volumes of mice from **B**. **D,** BLI quantification of mice from **B**. sr, steradian. **E,** The E0771-Luc2/GFP cell rechallenges are plotted alongside individual tumor growth data of E0771-Luc2/GFP implanted in naïve Tol mice from **Fig. 1C**; these experiments were not conducted side by side and are presented together only to aid in visualization and direct comparison. **A,** Created in BioRender. Khan, K. (2025) https://BioRender.com/k55g794.

visualized by CD31 and endomucin staining to provide information on tissue architecture. Polyclonal antibodies against luciferase could specifically identify tumor masses in the lungs and liver, with minimal reactivity in the normal lung or liver parenchyma (**Fig. 4A** and **B**). Necrotic cores were observed in the center of many large metastases (**Fig. 4B**), consistent with BLI imaging of large primary B16F1-Luc2/GFP tumors (Supplementary Fig. S4A).

Tol mice can facilitate the development of experimental brain metastasis models in this case of breast cancer

One of the most difficult circumstances to successfully treat in patients with cancer is brain metastases. To investigate the differences in tumor growth between WT and Tol mice within the brain and to establish an improved experimental brain metastasis model for future immunotherapy studies, we implanted E0771-Luc2/GFP cells intracranially and monitored tumor growth overtime (**Fig. 5A**). In some examples, tumors grew with an invasive front mixed with brain parenchyma (Supplementary Fig. S5A). In one representative experiment, BLI revealed signals in all Tol mice at seven DPI whereas the signal had depleted in two of four WT mice at this stage (**Fig. 5B**; Supplementary Fig. S5B). In some examples, tumors and BLI signal were observed away from the injection site (Supplementary Fig. S5C). By 14 DPI and beyond (up to 21 DPI), no BLI signal was detected in WT mice, whereas two of the four Tol mice showed high BLI signal. In the remaining

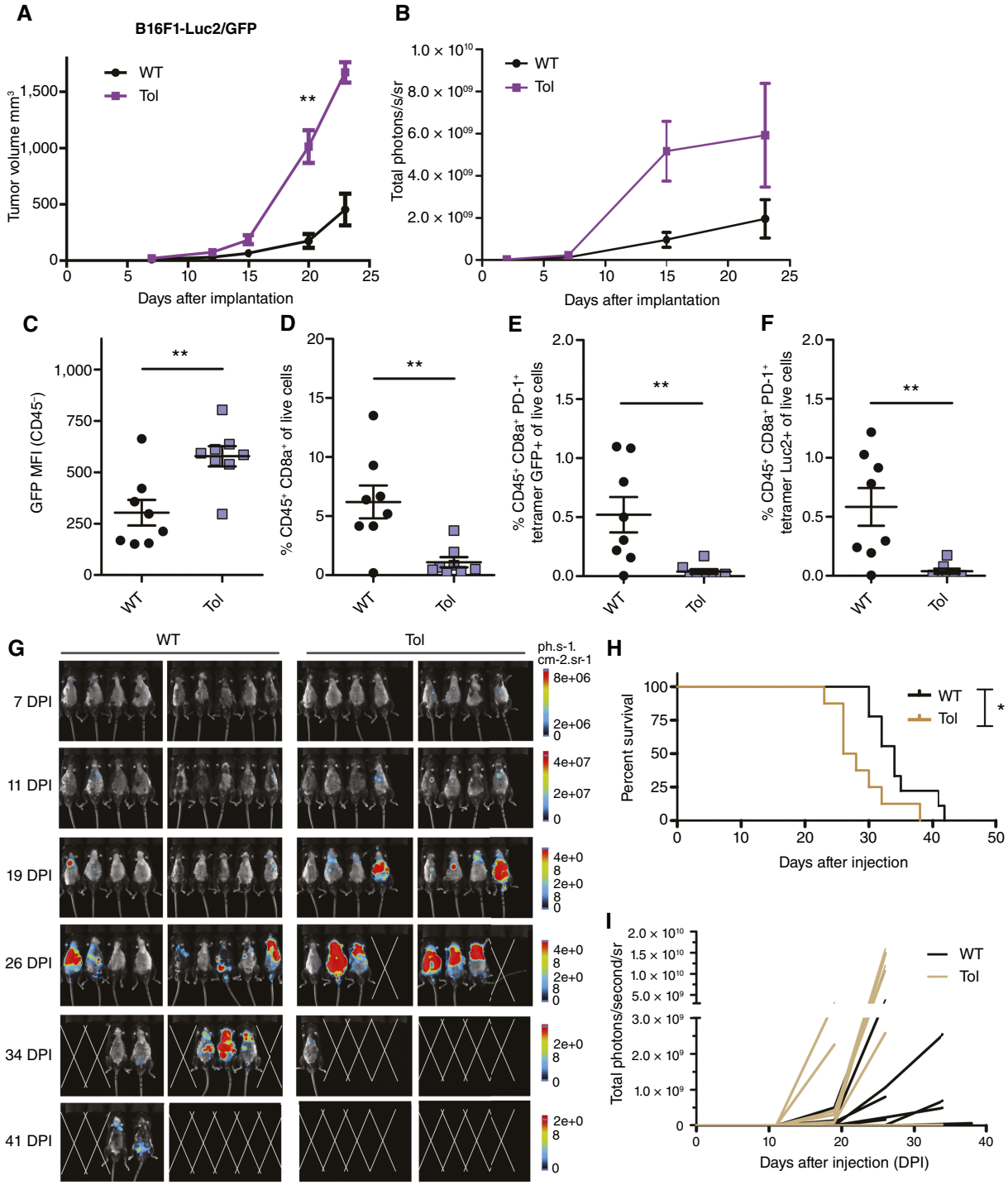

Figure 3.

Reduced growth of B16F1-Luc2/GFP cells in WT mice in comparison with Tol mice. **A,** Tumor volume of B16F1-Luc2/GFP implanted subcutaneously in WT vs. Tol mice. For 20 DPI, an unpaired *t* test was used, with **, $P = 0.0018$ and $n = 4$ per group. **B,** BLI of WT vs. Tol mice from **A**. **C,** B16F1-Luc2/GFP cells dissociated at 12 DPI were subjected to flow cytometry. GFP mean fluorescence intensity (MFI) of $CD45^-$ tumor cells was assessed by an unpaired *t* test, with **, $P = 0.0039$ and $n = 8$ per group. **D,** Percentage of $CD45^+$ $CD8a^+$ cells of total live cells as assessed by an unpaired *t* test. **, $P = 0.0035$. **E,** Percentage of $CD45^+$ $CD8a^+$ $PD\text{-}1^+$ GFP tetramer+ of total live cells as assessed by an unpaired *t* test. **, $P = 0.0067$. **F,** Percentage of $CD45^+$ $CD8a^+$ $PD\text{-}1^+$ Luc2 tetramer+ of total live cells as assessed by an unpaired *t* test. **, $P = 0.0045$. **G,** BLI images of mice intravenously injected with B16F1-Luc2/GFP, WT vs. Tol. **H,** Kaplan–Meier plot of survival analysis from **C**; a log-rank Mantel–Cox test was used. *, $P = 0.0261$; $P = 0.0261$. WT, $n = 9$; Tol, $n = 8$. **I,** BLI quantitation of mice from **D** and **E**. sr, steradian.

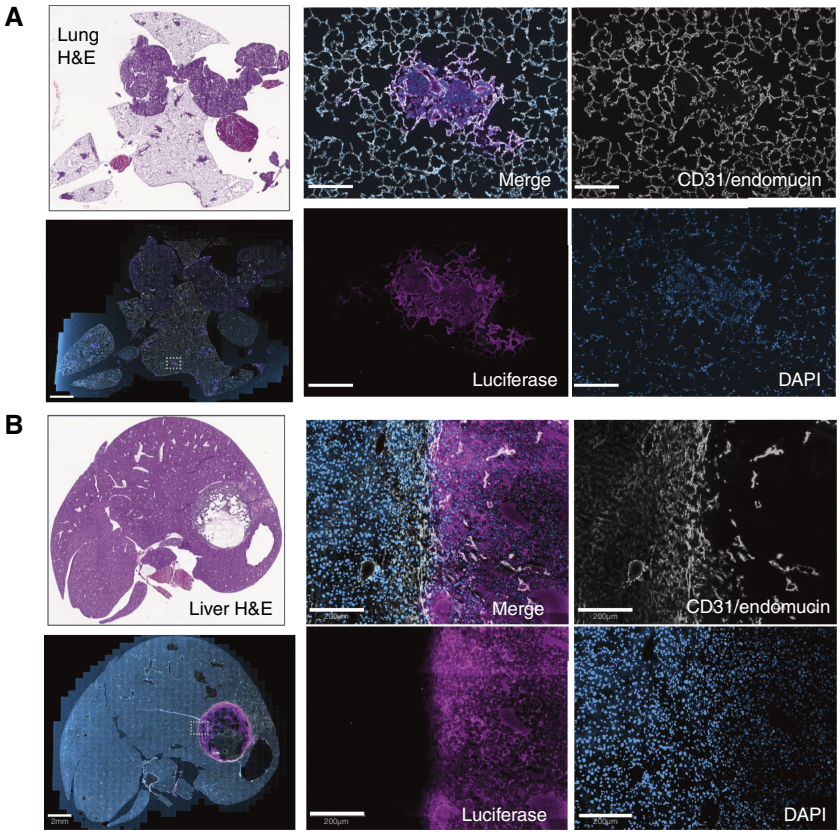

Figure 4.

Luciferase can be detected and utilized as a tumor-specific marker in Tol mice. **A,** Hematoxylin and eosin (H&E) and immunofluorescence imaging of lungs from recipient Tol mice that had been injected intravenously into the tail vein with B16F1-Luc2/GFP cells. **B,** Hematoxylin and eosin and immunofluorescence staining of the liver from Tol mice injected in the tail vein with B16F1-Luc2/GFP. Antibodies against luciferase (magenta) and CD31/endomucin vessels (gray) were used and DAPI was used to stain nuclei (blue). Scale bars on the full liver and lung represent 2 mm, whereas the separate panels are 200 μm.

two Tol mice, in which the BLI signal had depleted at 14 DPI, clinical symptoms and BLI reappeared at 74 and 75 DPIs (**Fig. 5B**; Supplementary Fig. S5D–S5F). This recurrence could represent a tumor subtype that has undergone adaptive changes within the brain microenvironment; therefore, we derived a tumor cell line from a brain lesion of one of these mice, which retained expression of GFP (Supplementary Fig. S5G). This variant cell line also displayed neural-like projections or "tumor microtubes" as has been described previously for brain cancers such as glioblastoma (27). In two experiments, in which overall survival was pooled, there was a significant reduction in survival of Tol mice compared with WT, with Tol displaying more tumor engraftment and eventual symptoms of brain metastasis (**Fig. 5C**). The presence of brain metastases in Tol mice was confirmed by histology and immunofluorescence staining using luciferase and GFP antibodies (**Fig. 5D**). In multiple examples, there was even metastasis within the brain, distant from the original injection point, possibly representing more metastatic and invasive variants (**Fig. 5D**; Supplementary Fig. S5C).

Postsurgical resection modeling of triple-negative breast cancer metastasis in Tol mice

To expand the number of cancer lines and models that can be used in Tol mice, we backcrossed C57Bl/6 Tol to BALB/c. We utilized sixth-generation BALB/c hybrid mice to test the development of primary tumors and metastasis from 4T1.2-Luc2/GFP cells orthotopically implanted in WT versus Tol mice. All mice showed positive BLI signal 1 day after mammary fat pad implantation; however, by 10 DPI, the WT mice had markedly reduced BLI signal and some had either completely rejected the primary tumor at this stage or completely lost BLI signal (**Fig. 6A**). At 15 DPI, primary tumors were surgically resected and the excised mammary fat pad and tumor were analyzed by *ex vivo* BLI. This revealed robust BLI signal in resections from Tol mice but lack of signal in WT mice (**Fig. 6B**). At the day of resection, WT tumor volume was significantly smaller than in Tol mice (Supplementary Fig. S6A). The day after resection, BLI revealed some residual signal likely pertaining to tumor nodules or cells that remained after surgical resection in Tol mice (**Fig. 6C**). At 29 DPI, the majority of Tol mice began to display distant metastases to lungs and lymph nodes and displayed dissemination in the opposite mammary fat pad. Additionally, some Tol mice displayed rarer metastases such as to the liver and bone, and variant lines could be derived from tumors at these sites (Supplementary Fig. S6B and S6C). Finally, upon endpoint, Tol mice showed robust BLI signal in metastases, whereas no signal was detected in WT mice even in mice that displayed tumor regrowth at the resection site or lung metastases. Immunofluorescence revealed luciferase staining in metastases from Tol mouse lungs, whereas minimal staining was observed in WT despite the presence of extensive metastases (Supplementary Fig. S7A and S7B). There was a significant difference in overall survival between Tol and WT mice; the median survival for Tol mice was 39 DPI whereas it was 102 DPI for WT mice and four of eight did not display any disease symptoms (**Fig. 6D**). In summary, Tol mice on the BALB/c background can be used to develop BLI-trackable cancer models, in which primary tumors are resected, more closely mimicking some clinical scenarios.

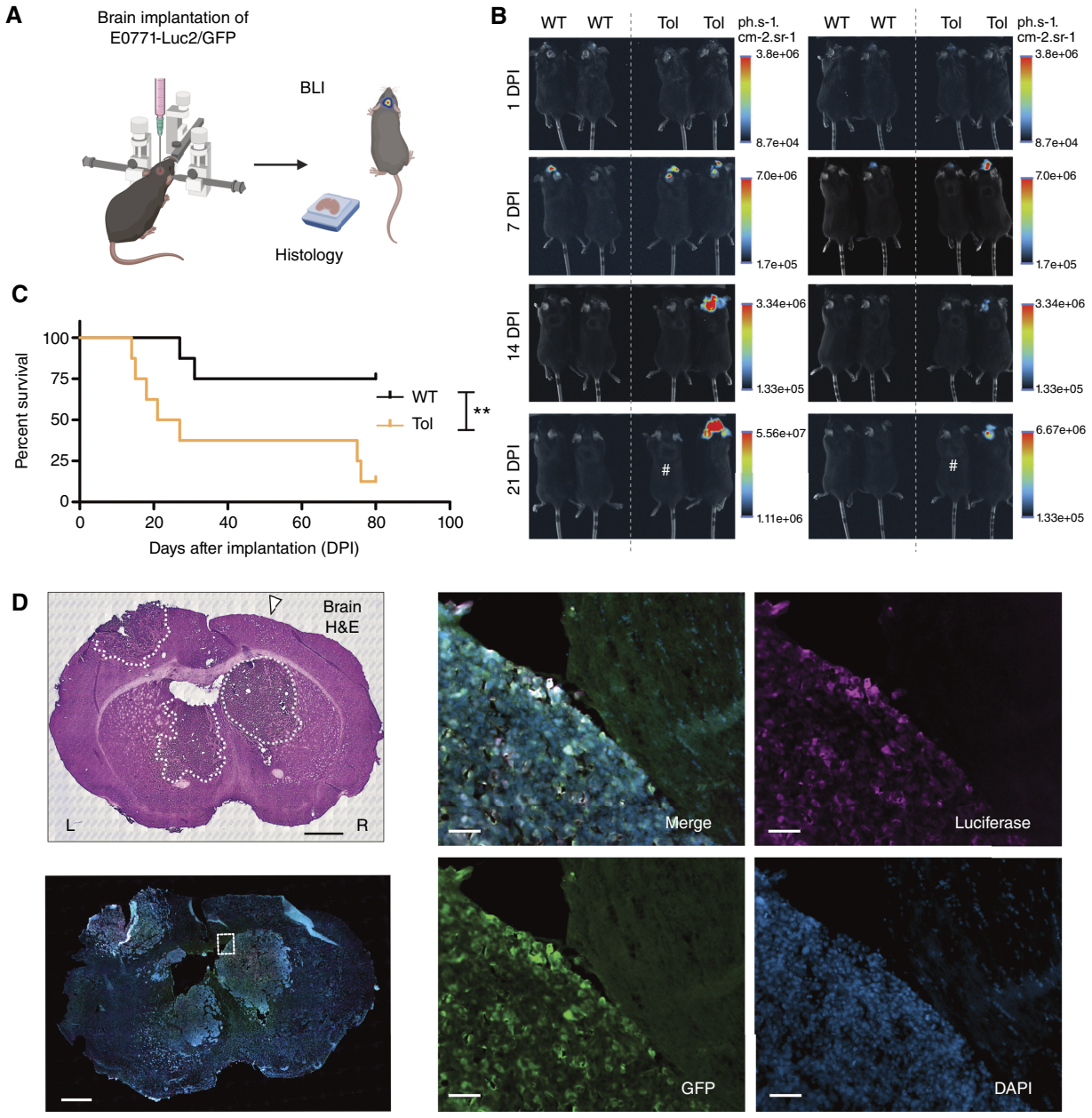

Figure 5.

E0771-Luc2/GFP tumor growth in the brain is maintained in Tol mice but rejected in the majority of WT mice. **A,** Schematic diagram of the brain implantation experiment. **B,** BLI of WT vs. Tol mice with brain implantation of E0771-Luc2/GFP cells. #, The two Tol mice in this figure that lost signal showed a recurrence of tumor growth at 74 and 75 DPI. **C,** Kaplan–Meier survival analysis of mice from **B**. A log-rank Mantel–Cox test was used, with **, $P = 0.0095$ and $n = 8$ per group. **D,** Hematoxylin and eosin (H&E) staining of a Tol mouse brain with the original injected tumor (arrowhead) and two metastases, L, left; R, right. Immunofluorescence images of a Tol mouse brain with luciferase (magenta) and GFP (green), colocalization (gray), and DAPI (blue). Whole brain scan, scale bar, 1 mm or 800 μm for hematoxylin and eosin or immunofluorescence, respectively. Inset image illustrates GFP- and luciferase-positive cells at the perimeter of the tumor. Scale bar, 50 μm. **A,** Created in BioRender. Khan, K. (2025) https://BioRender.com/t56m414.

Immune checkpoint blockade results in differential effects in WT versus Tol mice bearing B16F1-Luc2/GFP melanoma tumors

We hypothesized that because of the strong antigenic load of xenogeneic luciferase and GFP proteins, one of two scenarios could occur in WT mice but not in Tol mice. In the first scenario, tumor cells containing strong neoantigens must avoid the adaptive immune system early on in tumorigenesis and they may develop acquired mechanisms to evade adaptive immunity. In this circumstance, immunotherapy would likely be less effective in WT mice. In the second scenario, tumor cells expressing strong neoantigens will be recognized by $CD8^+$ T cells once immune evasion is relieved with immunotherapy in the form of

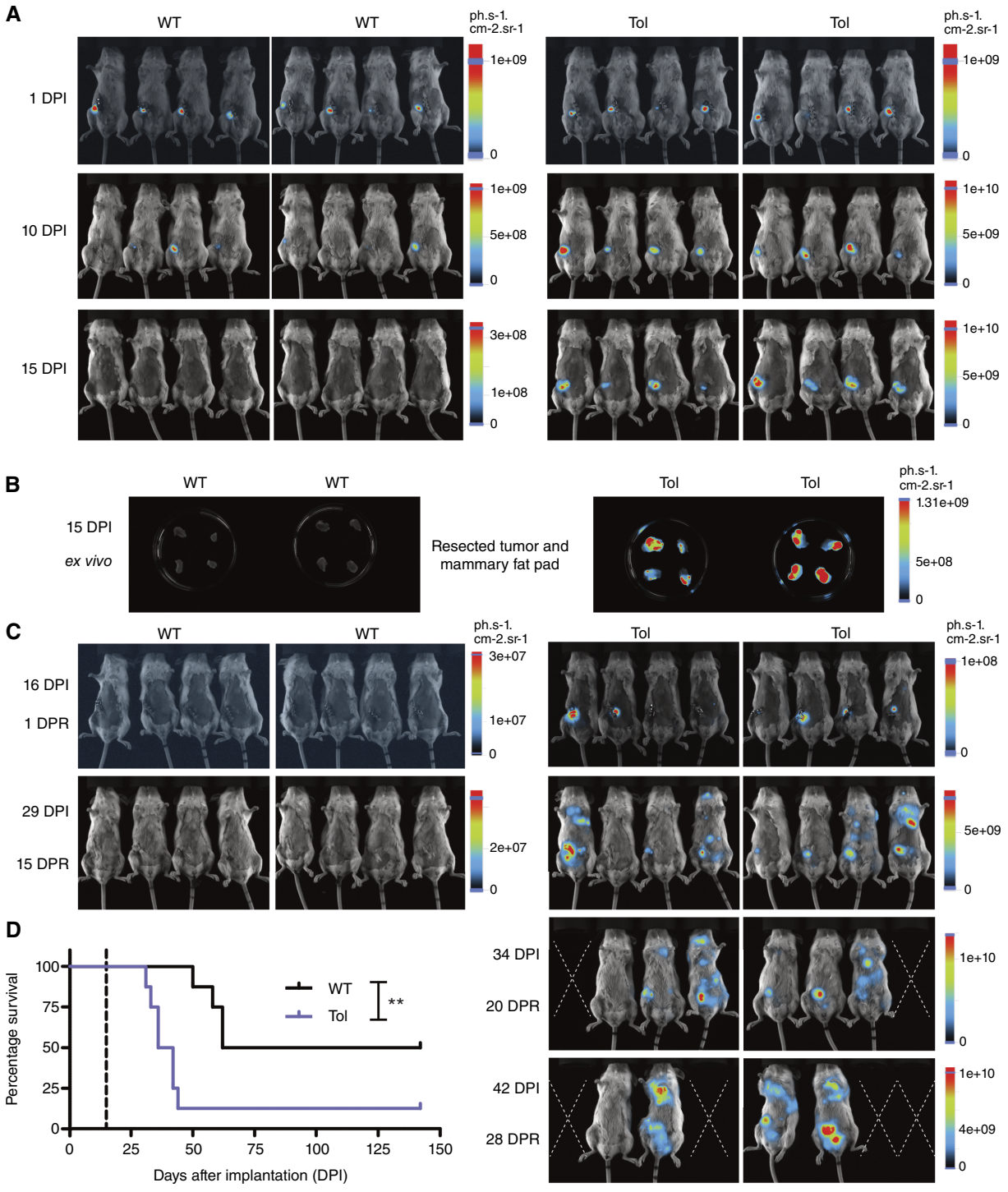

Figure 6.

Tol BALB/c mice can be used to generate post-resection models of 4T1.2-Luc2/GFP metastasis. **A,** BLI of WT vs. Tol mice implanted with 4T1.2-Luc2/GFP into the mammary fat pad, showing reduced signal in WT but signal maintenance in Tol mice. **B,** *Ex vivo* BLI of resected tumor and surrounding mammary fat pad in WT vs. Tol mice. **C,** BLI of WT vs. Tol mice after surgical resection of primary tumor shows BLI signal of metastasis developing in Tol mice but not in WT mice. **D,** Overall survival analysis of WT vs. Tol mice. Four of eight WT mice were euthanized for large regrowth at the site of resection but did not display BLI signal, whereas all Tol mice were euthanized for clinical symptoms of metastasis and displayed BLI in metastases. A log-rank Mantel–Cox was used, with **, $P = 0.0064$ and $n = 8$ per group. DPR, days post resection.

immune checkpoint inhibitor (ICI) antibody therapy, resulting in more robust effects. We chose to utilize the B16F1-Luc2/GFP model as at 12 days post implantation, tumors were of similar size between WT and Tol for treatment initiation (Supplementary Fig. S8A–S8C). We chose a doublet treatment regimen similar to immunotherapy for patients with melanoma in which a PD-1 antibody is given in combination with a CTLA4 antibody (28), followed by a period of maintenance PD-1 antibody blockade alone (**Fig. 7A**). Strikingly, WT mice treated with the ICIs were able to reject five of seven tumors initially (two of which relapsed against therapy), resulting finally in three of seven CRs (**Fig. 7B** and **C**). Interestingly, the relapsed tumors after ICI therapy displayed low BLI signal despite the tumors being of a large volume, potentially representing tumor cells that have undergone immune editing (Supplementary Fig. S8D and S8E). In contrast, in Tol mice, there were no clear effects on tumor growth (**Fig. 7B** and **D**; Supplementary Fig. S8F). At time points in which all mice in WT or Tol were present, there were significant differences in tumor volumes in WT undergoing ICI treatment, whereas no differences were observed in Tol mice treated with ICI (**Fig. 7E** and **F**). These mice were monitored until the tumor endpoint was reached as a surrogate survival study to

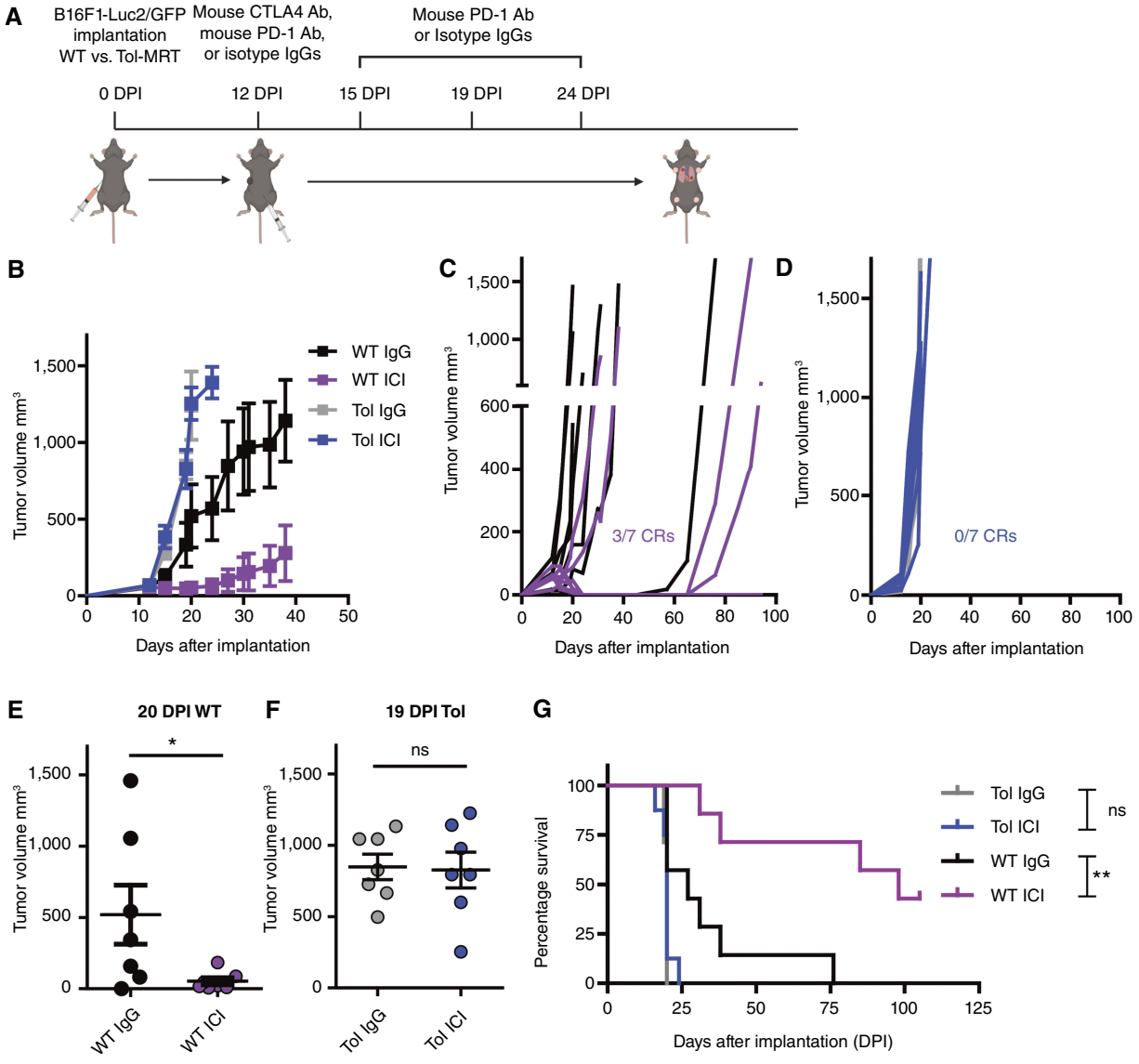

Figure 7.

Immune inhibition antibody therapy in mice bearing B16F1-Luc2/GFP results in efficacy only in WT mice. **A,** Schematic diagram of the experimental design. **B,** Mean tumor volume of WT vs. Tol mice treated with isotype control IgG or ICI with data cutoff at 40 DPI and $n = 7$ per group. **C,** Individual tumor growth observed in WT mice treated with IgG control or ICI showing some CRs. **D,** Individual tumor growth of Tol mice treated with IgG control or ICI showing no CRs. **E,** Tumor volume of WT mice at 20 days after implantation as assessed by an unpaired *t* test, with *, $P = 0.0443$ and $n = 7$ per group. **F,** Tumor volume of Tol mice at 19 days after implantation as assessed by an unpaired *t* test. ns, not significant; $P = 0.8887$. **G,** Kaplan–Meier survival plot of WT vs. Tol mice treated with IgG control vs. ICI. A log-rank Mantel–Cox test of WT IgG isotype vs. ICI, **, $P = 0.0030$; Tol IgG vs. Tol ICI, $P = 0.6465$; WT IgG vs. Tol IgG, *, $P = 0.0136$; and WT ICI vs. Tol ICI, with ***, $P = 0.0002$ and $n = 7$ per group. **A,** Created in BioRender. Khan, K. (2025) https://BioRender.com/u83x866.

determine the extent of CRs. There were significant differences in overall survival for WT mice treated with ICIs, whereas there was no difference in Tol mice treated with ICIs (**Fig. 7G**). The lack of response in Tol mice is unsurprising as similar findings have been reported with parental B16 cells implanted in WT mice poorly responding to CTLA4 and PD-1 antibody blockade (29). This demonstrates that luciferase and GFP are strong neoantigens that render the tumor cells sensitive to ICI therapy in WT mice, an effect that is lost when mice are immunologically tolerant and detect these reporter proteins as self-antigens.

Discussion

Our study demonstrates that Tol mice are an additional model to address the widespread problem of immunogenic transgenes and their use in tumor models (13, 30, 31). We demonstrate that in certain tumor models, such as the E0771 breast cancer cell line, coexpression of luciferase and GFP leads to complete rejection in WT mice when implanted in the mammary fat pad, whereas Tol mice, immunologically tolerant to both proteins, exhibit progressive tumor growth. The use of Tol mice allows for the generation of BLI traceable models of E0771 in the mammary fat pad and brain. This will likely also be the case for many other cell lines that would undergo similar fates of rejection if grown in immunocompetent WT mice and thus would expand the number of models that can be investigated in immunocompetent mice using BLI analyses. We also report that cell lines such as the B16F1 melanoma line can grow in WT mice when expressing Luc2 and GFP, which has been reported previously (29, 32, 33); however, growth occurs at a slower rate than in Tol mice. Therefore, such a difference in the growth rate may have been overlooked in other studies using this widely employed cell line. We also show that GFP- and luciferase-specific $CD8^+$ T cells are detectable in B16F1-Luc2/GFP tumors from WT mice compared with much lower levels in Tol mice. We propose that even in cases in which tumors expressing luciferase and GFP do not undergo complete rejection in WT mice (as seen with B16F1), there is still a clear adaptive immune response invoked against these highly immunogenic xenogeneic proteins, which can be unleashed and amplified using ICI therapy. This raises the risk of overestimating the antitumor efficacy of such immunotherapies, especially in tumor types that do not contain a high number of endogenous mutations, which lead to the expression of neoantigens that $CD8^+$ T cells can recognize. Clinical tumor counterparts with low mutational burden include pancreatic cancer, breast cancer, prostate cancer, and glioblastoma, among others (34, 35). We cannot rule out whether the same ICI-mediated effects would be seen if cells were expressing GFP or luciferase alone, but this would be an interesting future study. Finally, we demonstrate the capability of generating BLI-traceable postsurgical resection models. Such a strategy can allow different experimental treatment settings such as prior to surgery (neoadjuvant therapy), after surgery (adjuvant therapy), or when treating advanced metastatic disease, something that would not be possible to determine without imaging relative disease burden.

The use of so-called "glowing head" mice has been suggested as a way to allow implantation of both Luc2- and GFP-positive cells to avoid immunogenicity as both genes are expressed in the pituitary gland (12). However, more recent studies have demonstrated that these mice do not display robust tolerance to Luc2 and GFP expressed in tumor cells (13, 30). Additionally, glowing head mice do not give rise to metastases despite the use of highly metastatic 4T1 breast cancer cells (13). Other inventive ways to circumvent the problem of immunogenic transgenes have been reported, such as the use of transgenic mice that express GFP in dendritic cells (DC) and therefore present GFP as self-peptides to the adaptive immune system (13, 36). However, there are some caveats with this approach, such as limitations on the number and types of genes that have been engineered to be expressed in DCs (under the control of the chemokine receptor *Cx3cr1* promoter) and also the fact that DCs as well as monocytes, microglia, and NK cells will express the transgene of interest (37), potentially complicating imaging and downstream analyses. The third reported approach involves the use of transgenic mice that express nonfluorescent or enzymatically inactive forms of GFP or luciferase, respectively (31). The recent creation of "NoGlow" mice, which combined inactive forms of luciferase and GFP, allowing for *in vivo* BLI and *ex vivo* fluorescence imaging, is another important advance (30). However, it remains to be seen whether NoGlow mice offer the same advantages as Tol mice for immunotherapy studies. Additionally, although not examined in this study, an additional advantage of the Tol mice is tolerance to Cre recombinase and multiple fluorescent reporters in addition to GFP. The latter could, for example, allow for designing cell competition experiments modeling tumor heterogeneity to study the response of two or more cancer cell lines to immunotherapy – something not possible in other tolerant mice.

It is clear from our studies that the contribution of immunogenicity of luciferase and GFP may vary between tumor models. We speculate that each model will fall into one of the following three scenarios: (i) tumors are completely rejected, (ii) undergo an underlying immune response that can be reinvigorated with ICIs (such as PD-1 or PD-L1 antibodies), or (iii) have no effect on growth or metastasis between WT and Tol mice. The third category could represent tumor lines that are intrinsically resistant to the adaptive immune system and may, for instance, have defects in MHC class I antigen presentation (38). In the future, we plan to use Tol mice to generate additional orthotopic tumor models of different types for ICI therapy and metastasis studies.

A major benefit of BLI usage in preclinical cancer models lies in the ability to track the progression of tumors in organs deep in the body; however, even primary tumors at the surface that would normally be measured with calipers can benefit from BLI. For example, in our ICI experiments, complete tumor regressions were observed in several WT mice and the tumor was not palpable but eventually showed weak BLI signal (Supplementary Fig. S8D). Indeed, with continued imaging of these animals, local tumor recurrences occurred, which, importantly, were found to be unresponsive to re-initiated ICI therapy. Therefore, there is clear utility in BLI use for the tracing of many tumor types in preclinical models and could lead to the development and isolation of therapy-resistant variants, as well as the potential for facilitating studies on the phenomenon of tumor dormancy.

The use of GFP as a co-marker of successful transduction has multiple uses. First, it can be used in flow cytometry applications to better identify tumor cells as robust and specific tumor markers are currently lacking in many preclinical mouse tumor lines and models. Second, it can be used to follow individual tumor cells through intravital microscopy (39, 40). Third, GFP can be used to determine and purify tumor cells after derivation of new variant lines after *in vivo* growth. Finally, GFP can be used to ensure a pure but heterogeneous population of tumor cells that are successfully transduced with the transgenes of interest before being introducing into mice (Supplementary Fig. S9A–S9C). The maintenance of a heterogeneous population better representing the parental cell line could be critical as the alternative may involve clonal selection, which could select for clones that are more or less responsive to therapies in comparison with the original cell line. Additionally, such an approach likely allows

maintenance of characteristics of the original line including tumorigenicity and metastatic potential. In other words, selection of hundreds of thousands of cells by sorting for GFP allows for a better representation of the original cell line, resulting in better comparisons across studies and experiments from different research laboratories. The latter point is a key consideration in the ongoing reproducibility crisis involving preclinical modeling of cancer biology (41, 42). We acknowledge that the dual expression of GFP alongside luciferase may increase the immunogenicity of cells more than either transgene alone. However, at least in C57Bl/6 mice, GFP has been described as a weak antigen (43, 44). In the BALB/c background, the immunogenicity of GFP may have more relevance (13), a problem that will likely be mitigated with the use of the Tol mice.

In summary, we propose the use of Tol mice for studies involving orthotopic implantation of tumors not amenable to physical measurements, as well as studies involving metastasis, especially in experiments involving tumor immunotherapy. Additionally, Tol mice will likely have utility in a broader research context such as immunology, neurobiology, and regenerative medicine among others.

Authors' Disclosures

No disclosures were reported.

Authors' Contributions

K.A. Khan: Conceptualization, data curation, formal analysis, supervision, validation, investigation, visualization, methodology, writing–original draft, writing–review and editing. **A.A. Qureshi:** Validation, investigation, methodology, writing–review and editing. **P. Xu:** Validation, investigation, methodology, writing–review and editing. **H.-Y. Kuo:** Investigation, writing–review and editing. **T.N. Schumacher:** Resources, writing–review and editing. **I.P. Michael:** Conceptualization, supervision, funding acquisition, writing–review and editing. **R.S. Kerbel:** Conceptualization, resources, supervision, funding acquisition, writing–review and editing.

Acknowledgments

We thank Dr. Kaspar Bresser and Colin Pritchard for advice regarding the development of the Tol mouse colony. We thank Dr. Katarzyna Jerzak for providing comments on the manuscript, Shan Man for expertise in surgeries and tumor implantation, and Stephanie White for cell irradiation. We thank Dr. Zeinab Noroozian and Andrew Nicholson of Dr. Isabelle Aubert's lab for guidance in brain implantation experiments. Our thanks are also extended to: Sunnybrook Histology core facility (Petia Stefanova), The Centre for Flow Cytometry & Scanning Microscopy (Kevin Conway and Paul Oleynik), and Comparative Research and the Toronto Centre for Phenogenomics for their vital core services. Finally, we thank Cassandra Cheng for excellent secretarial assistance. This work was supported by a grant to R.S. Kerbel from the Canadian Institute of Health Research (CIHR). K.A. Khan was supported by a CIHR Banting Postdoctoral Fellowship award. This work was also supported by the Terry Fox New Frontiers Program Project Grant to I.P. Michael (TFRI project #1124). Research in the I.P. Michael laboratory is supported by Canadian Foundation for Innovation John R. Evans Leaders Fund grant and CIHR project grant (497392). I.P. Michael is supported by a Tier 2 Canadian Research Chair.

Note

Supplementary data for this article are available at Cancer Research Online (http://cancerres.aacrjournals.org/).

Received July 15, 2024; revised December 12, 2024; accepted April 8, 2025; posted first April 14, 2025.

References

1. Upadhaya S, Neftelinov ST, Hodge J, Campbell J. Challenges and opportunities in the PD1/PDL1 inhibitor clinical trial landscape. Nat Rev Drug Discov 2022;21:482–3.
2. Boshuizen J, Peeper DS. Rational cancer treatment combinations: an urgent clinical need. Mol Cell 2020;78:1002–18.
3. Hegde PS, Chen DS. Top 10 challenges in cancer immunotherapy. Immunity 2020;52:17–35.
4. Gengenbacher N, Singhal M, Augustin HG. Preclinical mouse solid tumour models: status quo, challenges and perspectives. Nat Rev Cancer 2017;17:751–65.
5. Francia G, Cruz-Munoz W, Man S, Xu P, Kerbel RS. Mouse models of advanced spontaneous metastasis for experimental therapeutics. Nat Rev Cancer 2011;11:135–41.
6. Zhang L, Hellström KE, Chen L. Luciferase activity as a marker of tumor burden and as an indicator of tumor response to antineoplastic therapy in vivo. Clin Exp Metastasis 1994;12:87–92.
7. Gambotto A, Dworacki G, Cicinnati V, Kenniston T, Steitz J, Tüting T, et al. Immunogenicity of enhanced green fluorescent protein (EGFP) in BALB/c mice: identification of an H2-Kd-restricted CTL epitope. Gene Ther 2000;7:2036–40.
8. Han WGH, Unger WWJ, Wauben MHM. Identification of the immunodominant CTL epitope of EGFP in C57BL/6 mice. Gene Ther 2008;15:700–1.
9. Limberis MP, Bell CL, Wilson JM. Identification of the murine firefly luciferase-specific CD8 T-cell epitopes. Gene Ther 2009;16:441–7.
10. Stripecke R, Carmen Villacres M, Skelton D, Satake N, Halene S, Kohn D. Immune response to green fluorescent protein: implications for gene therapy. Gene Ther 1999;6:1305–12.
11. Steinbauer M, Guba M, Cernaianu G, Köhl G, Cetto M, Kunz-Schughart LA, et al. GFP-transfected tumor cells are useful in examining early metastasis in vivo, but immune reaction precludes long-term tumor development studies in immunocompetent mice. Clin Exp Metastasis 2003;20:135–41.
12. Day C-P, Carter J, Weaver Ohler Z, Bonomi C, El Meskini R, Martin P, et al. "Glowing head" mice: a genetic tool enabling reliable preclinical image-based evaluation of cancers in immunocompetent allografts. PLoS One 2014;9:e109956.
13. Grzelak CA, Goddard ET, Lederer EE, Rajaram K, Dai J, Shor RE, et al. Elimination of fluorescent protein immunogenicity permits modeling of metastasis in immune-competent settings. Cancer Cell 2022;40:1–2.
14. Ferrari DP, Ramos-Gomes F, Alves F, Markus MA. KPC-luciferase-expressing cells elicit an anti-tumor immune response in a mouse model of pancreatic cancer. Sci Rep 2024;14:13602.
15. Huang L, Bommireddy R, Munoz LE, Guin RN, Wei C, Ruggieri A, et al. Expression of tdTomato and luciferase in a murine lung cancer alters the growth and immune microenvironment of the tumor. PLoS One 2021;16:e0254125.
16. Baklaushev VP, Kilpeläinen A, Petkov S, Abakumov MA, Grinenko NF, Yusubalieva GM, et al. Luciferase expression allows bioluminescence imaging but imposes limitations on the orthotopic mouse (4T1) model of breast cancer. Sci Rep 2017;7:7715.
17. Bresser K, Dijkgraaf FE, Pritchard CEJ, Huijbers IJ, Song J-Y, Rohr JC, et al. A mouse model that is immunologically tolerant to reporter and modifier proteins. Commun Biol 2020;3:273.
18. Lelekakis M, Moseley JM, Martin TJ, Hards D, Williams E, Ho P, et al. A novel orthotopic model of breast cancer metastasis to bone. Clin Exp Metastasis 1999;17:163–70.
19. Hopert A, Uphoff CC, Wirth M, Hauser H, Drexler HG. Mycoplasma detection by PCR analysis. In Vitro Cell Dev Biol Anim 1993;29A:819–21.
20. Noy PJ, Swain RK, Khan K, Lodhia P, Bicknell R. Sprouting angiogenesis is regulated by shedding of the C-type lectin family 14, member A (CLEC14A) ectodomain, catalyzed by rhomboid-like 2 protein (RHBDL2). FASEB J 2016;30:2311–23.
21. Wu FTH, Xu P, Chow A, Man S, Krüger J, Khan KA, et al. Pre- and post-operative anti-PD-L1 plus anti-angiogenic therapies in mouse breast or renal cancer models of micro- or macro-metastatic disease. Br J Cancer 2019;120:196–206.
22. Khan KA, Ponce de Léon JL, Benguigui M, Xu P, Chow A, Cruz-Muñoz W, et al. Immunostimulatory and anti-tumor metronomic cyclophosphamide regimens assessed in primary orthotopic and metastatic murine breast cancer. NPJ Breast Cancer 2020;6:29.

23. Müller-Kuller U, Ackermann M, Kolodziej S, Brendel C, Fritsch J, Lachmann N, et al. A minimal ubiquitous chromatin opening element (UCOE) effectively prevents silencing of juxtaposed heterologous promoters by epigenetic remodeling in multipotent and pluripotent stem cells. Nucleic Acids Res 2015;43: 1577–92.
24. Chen IX, Newcomer K, Pauken KE, Juneja VR, Naxerova K, Wu MW, et al. A bilateral tumor model identifies transcriptional programs associated with patient response to immune checkpoint blockade. Proc Natl Acad Sci U S A 2020;117:23684–94.
25. Crosby EJ, Wei J, Yang XY, Lei G, Wang T, Liu C-X, et al. Complimentary mechanisms of dual checkpoint blockade expand unique T-cell repertoires and activate adaptive anti-tumor immunity in triple-negative breast tumors. Oncoimmunology 2018;7:e1421891.
26. Kuczynski EA, Krueger J, Chow A, Xu P, Man S, Sundaravadanam Y, et al. Impact of chemical-induced mutational load increase on immune checkpoint therapy in poorly responsive murine tumors. Mol Cancer Ther 2018;17: 869–82.
27. Osswald M, Jung E, Sahm F, Solecki G, Venkataramani V, Blaes J, et al. Brain tumour cells interconnect to a functional and resistant network. Nature 2015; 528:93–8.
28. Hodi FS, Chesney J, Pavlick AC, Robert C, Grossmann KF, McDermott DF, et al. Combined nivolumab and ipilimumab versus ipilimumab alone in patients with advanced melanoma: 2-year overall survival outcomes in a multicentre, randomised, controlled, phase 2 trial. Lancet Oncol 2016;17:1558–68.
29. Curran MA, Montalvo W, Yagita H, Allison JP. PD-1 and CTLA-4 combination blockade expands infiltrating T cells and reduces regulatory T and myeloid cells within B16 melanoma tumors. Proc Natl Acad Sci U S A 2010; 107:4275–80.
30. Trotter TN, Wilson A, McBane J, Dagotto CE, Yang X-Y, Wei J-P, et al. Overcoming xenoantigen immunity to enable cellular tracking and gene regulation with immune-competent "NoGlow" mice. Cancer Res Commun 2024; 4:1050–62.
31. Aoyama N, Miyoshi H, Miyachi H, Sonoshita M, Okabe M, Taketo MM. Transgenic mice that accept Luciferase- or GFP-expressing syngeneic tumor cells at high efficiencies. Genes Cells 2018;23:580–9.
32. Tiffen JC, Bailey CG, Ng C, Rasko JEJ, Holst J. Luciferase expression and bioluminescence does not affect tumor cell growth in vitro or in vivo. Mol Cancer 2010;9:299.
33. Craft N, Bruhn KW, Nguyen BD, Prins R, Liau LM, Collisson EA, et al. Bioluminescent imaging of melanoma in live mice. J Invest Dermatol 2005; 125:159–65.
34. Imamura T, Ashida R, Ohshima K, Uesaka K, Sugiura T, Ohgi K, et al. Characterization of pancreatic cancer with ultra-low tumor mutational burden. Sci Rep 2023;13:4359.
35. Li M, Gao X, Wang X. Identification of tumor mutation burden-associated molecular and clinical features in cancer by analyzing multi-omics data. Front Immunol 2023;14:1090838.
36. Schultheiß C, Binder M. Overcoming unintended immunogenicity in immunocompetent mouse models of metastasis: the case of GFP. Signal Transduct Target Ther 2022;7:68.
37. Jung S, Aliberti J, Graemmel P, Sunshine MJ, Kreutzberg GW, Sher A, et al. Analysis of fractalkine receptor CX(3)CR1 function by targeted deletion and green fluorescent protein reporter gene insertion. Mol Cell Biol 2000;20:4106–14.
38. Dhatchinamoorthy K, Colbert JD, Rock KL. Cancer immune evasion through loss of MHC class I antigen presentation. Front Immunol 2021;12:636568.
39. Zhang Y, Toneri M, Ma H, Yang Z, Bouvet M, Goto Y, et al. Real-time GFP intravital imaging of the differences in cellular and angiogenic behavior of subcutaneous and orthotopic nude-mouse models of human PC-3 prostate cancer. J Cell Biochem 2016;117:2546–51.
40. Hoffman RM. Application of GFP imaging in cancer. Lab Invest 2015;95: 432–52.
41. Errington TM, Mathur M, Soderberg CK, Denis A, Perfito N, Iorns E, et al. Investigating the replicability of preclinical cancer biology. Elife 2021;10: e71601.
42. Errington TM, Denis A, Perfito N, Iorns E, Nosek BA. Challenges for assessing replicability in preclinical cancer biology. Elife 2021;10:e67995.
43. Denaro M, Oldmixon B, Patience C, Andersson G, Down J. EGFP-transduced EL-4 cells from tumors in C57BL/6 mice. Gene Ther 2001;8:1814–5.
44. Skelton D, Satake N, Kohn DB. The enhanced green fluorescent protein (eGFP) is minimally immunogenic in C57BL/6 mice. Gene Ther 2001;8:1813–4.